

INTERFACES. A Program for Determining the 3D Structures of Surface Sites Using NMR Data

James Cunningham¹ and Frédéric A. Perras¹

¹US DOE, Ames National Laboratory, Ames, IA 50011, USA

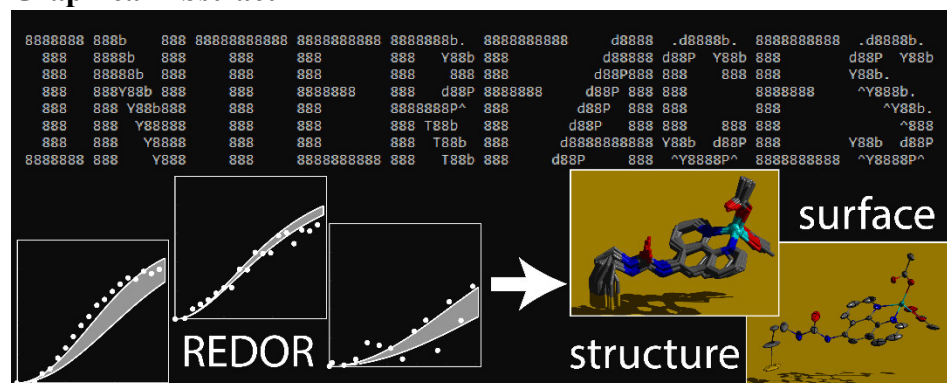
Highlights

- An open-source program, INTERFACES, is presented for the determination of the three-dimensional structure of surface sites
- The program automatically analyzes and fits molecular structures to various kinds of RE(SP)DOR data
- We describe how to build the input files necessary to use INTERFACES
- Structure determinations from the literature are reproduced

Abstract

Dynamic nuclear polarization surface enhanced NMR spectroscopy has enabled the determination of high-resolution structures from surface-supported molecules, including single-site heterogeneous catalysts. Structure determinations have largely mimicked the approaches used in biomolecular NMR spectroscopy, namely, using distance measurements to constrain a conformational search. These early demonstrations made use of purpose-built software, which has limited the adoption of the technique. Herein, we describe the open-source program INTERFACES (Interpret NMR to Elucidate or Reconstruct the Full Atomistic Configurations of External Surfaces) which automates the analysis of RE(SP)DOR data as well as the structure determination for surface sites. Distances, angles, dihedral angles, complex orientation, and distance from the support can all be sampled to find all structures that agree with the experimental data. A χ^2 metric is used to define the error ranges of the REDOR fits and produce structures with an arbitrary level of confidence. Structural solutions are then provided as both overlays and ORTEP-like probability ellipsoids.

Graphical Abstract



Keywords

Solid-State NMR, REDOR, Dynamic Nuclear Polarization, Structure Determination, Surface Science, Heterogeneous Catalysis

1. Introduction

The surfaces and interfaces of materials are often critical in defining their properties but are seldom characterized to the level that we are accustomed to seeing in molecular and crystalline systems. Of particular interest is the determination of the precise structures of catalytic active sites, which may yield mechanistic insights that could be leveraged for the design of new chemical reactions, or catalytic sites with enhanced activity or selectivity.¹⁻⁶

The difficulty in characterizing surface sites primarily stems from the facts that: 1) they are incredibly dilute, often only consisting of a fraction of a percent of the mass of a sample, and 2) surfaces and interfaces are generally disordered. Sparsely populated surface sites do not diffract, their light atoms are largely invisible in electron microscopy, and they elicit extremely weak nuclear magnetic resonance (NMR) signals. Their characterization has primarily been limited to the use of chemical tools, such as titrations, X-ray absorption spectroscopy, and spectroscopic methods (infrared, Raman, UV/vis, 1D NMR) that yield little spatial insights. The recent advent of dynamic nuclear polarization (DNP) surface enhance NMR spectroscopy (SENS)⁷⁻¹⁰ has, however, made it possible to routinely perform multidimensional NMR experiments on surfaces sites,¹¹⁻¹⁷ and even detect metal centers directly.¹⁸⁻²⁰ Most critically, however, DNP SENS has enabled for the measurement of both internuclear and surface-to-atom distances in supported metal complexes and revealed the first truly high-resolution structures of surface sites.²¹⁻²⁴ Recent work also suggests that obtaining similar details may be possible without DNP through the use of fast magic angle spinning (MAS) and ¹H detection,²⁵⁻²⁷ or isotope enrichment.²⁸

While the first surface structure determinations occurred over 5 years ago, very few structures have been determined,²¹ including Sc,²³ Zn,²³ Ag,²⁴ Ir,^{22,24} and Pt²¹ complexes. Part of the reasons for this slow adoption has been the limited availability of magic angle spinning (MAS)-DNP instrumentation and the more stringent sample preparation requirements. In addition, the lack of widely available software for solving such structures has been a large barrier for entry. To address this latter problem, we have written a program to automate the structure determination of surface sites using rotational-echo double-resonance (REDOR),²⁹ rotational-echo saturation-pulse double-resonance (RESPDOR),³⁰ or other data, such as extended X-ray absorption fine structure (EXAFS). The program, called INTERFACES (Interpret NMR to Elucidate or Reconstruct the Full Atomistic Configurations of External Surfaces), uses a distance geometry approach³¹ to modify an initial structure to maximize the agreement with the provided data. This paper will describe the functioning of the program, how to build an INTERFACES input file, and, lastly, we will use it to reproduce the results from five literature examples. These examples are available, together with the source code, on a Github repository.

2. Theory

Solid-state NMR-based distance measurements are generally performed using one of four closely related experiments, namely, the REDOR²⁹ and RESPDOR³⁰ experiments and their symmetry-based (S) counterparts: S-REDOR and S-RESPDOR.³² All four pulse sequences take the same general form, depicted in Figure 1, wherein a Hahn echo is performed on one channel, a zero-quantum heteronuclear dipolar recoupling sequence is applied to either channel during the

echo delays, and a perturbation pulse is applied to the non-detected nuclei. In the case of REDOR experiments the perturbation pulse is an inversion pulse while it is a saturation pulse in RESPDOR experiments. For optimal saturation in a RESPDOR experiment, it is generally recommended to apply Nimerovsky et al.'s phase-modulated saturation pulse.³³ Experiments are performed in pairs, with one of the two experiments neglecting the perturbation pulse in order to act as a reference. The reference signal is typically labelled as S_0 while the dipolar-dephased signal is labelled as S . Data are most often normalized to compensate for transverse relaxation as: $(S_0 - S)/S_0$, or more simply: $\Delta S/S_0$. $\Delta S/S_0$ is measured as a function of the total dipolar recoupling time, τ_{rec} , and grows at a rate that is proportional to the dipolar coupling constant (D) squared. D is given by the following expression and depends solely on the internuclear distance (r) and some fundamental constants, enabling the measurement of precise internuclear distances.

$$D = \frac{\mu_0}{4\pi} \frac{\hbar\gamma_1\gamma_2}{2\pi} \langle r^{-3} \rangle \quad (1)$$

In the equation above, μ_0 is the permeability of free space, γ_i is the gyromagnetic ratio of spin i , and \hbar is the reduced Plank constant.

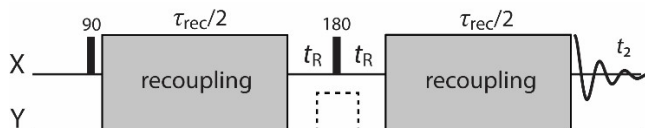


Figure 1. General RE(SP)DOR pulse sequence. In the case of REDOR the dashed pulse is an inversion pulse while it is a saturation pulse in RESPDOR. The recoupling sequence can be applied to either channel. t_R corresponds to the rotor period, minus half the width of the central X inversion pulse.

S-REDOR and S-RESPDOR³² generally refers to sequences that apply an $m=2$ symmetry-based dipolar recoupling sequence,³⁴ most often $SR4_1^2$,³⁵ to simultaneously perform homonuclear decoupling and heteronuclear recoupling. Their dipolar scaling factors are nearly halved and as such the regular REDOR and RESPDOR sequences are preferred when possible. RESPDOR sequences are most effective when the recoupled nuclei are quadrupolar (i.e. they have spin quantum numbers, $I > 1/2$) and REDOR produces twice the dephasing as RESPDOR when the recoupled spins have $I = 1/2$.

The REDOR dephasing is given by the following expression:³⁶

$$\frac{\Delta S}{S_0} = 1 - \frac{1}{4\pi} \int_0^{2\pi} \int_0^\pi \cos(2\sqrt{2}D\tau_{\text{rec}}\sin 2\beta\sin\alpha) \sin\beta d\alpha d\beta, \quad (2)$$

where α and β are the polar angles that define the orientation of an internuclear vector with respect to the rotation axis. This expression assumes complete dephasing, which is not always the case due to differences in isotopic abundance, heterogeneity, or pulse imperfections. As such, a contribution factor, f , is often included to compensate for these effects.

$$\frac{\Delta S}{S_0} = 1 - \frac{f}{4\pi} \int_0^{2\pi} \int_0^\pi \cos(2\sqrt{2}D\tau_{\text{rec}}\sin 2\beta\sin\alpha) \sin\beta d\alpha d\beta \quad (3)$$

In the event that dynamics may affect the magnitude of the recoupled dipolar interactions,

an order parameter, $\langle S \rangle$, can be used.

$$\frac{\Delta S}{S_0} = 1 - \frac{f}{4\pi} \int_0^{2\pi} \int_0^\pi \cos(2\sqrt{2}D\langle S \rangle \tau_{\text{rec}} \sin 2\beta \sin \alpha) \sin \beta d\alpha d\beta \quad (4)$$

If the REDOR experiment is performed to recouple half-integer quadrupolar nuclei, then generally the inversion pulse is central transition selective. As such, dipolar interactions to nuclei in one of the $|m| \neq 1/2$ states are not recoupled and f is reduced to a maximum value of $1/(I + 1/2)$. By applying a saturation pulse instead of a central transition selective pulse, i.e. a RESPDOR experiment, we can involve more of the nuclei and as such the dephasing is stronger. For instance, the REDOR signal when the recoupled nucleus is a spin-3/2 nuclide is:³²

$$\frac{\Delta S}{S_0} = 1 - \frac{f}{4\pi} \int_0^{2\pi} \int_0^\pi \left[\begin{array}{l} 1/4 + 3/8 \cos(2\sqrt{2}D\langle S \rangle \tau_{\text{rec}} \sin 2\beta \sin \alpha) \\ + 1/4 \cos(4\sqrt{2}D\langle S \rangle \tau_{\text{rec}} \sin 2\beta \sin \alpha) \\ + 1/8 \cos(6\sqrt{2}D\langle S \rangle \tau_{\text{rec}} \sin 2\beta \sin \alpha) \end{array} \right] \sin \beta d\alpha d\beta \quad (5)$$

where we assume an equal probability of magnetization exchange over the 4 0Q coherences, 6 1Q coherences, 4 2Q coherences, and 2 3Q coherences. Notice that the dipolar dephasing rate is proportional to Δm and as such RESPDOR not only leads to more pronounced dephasing, but also faster dephasing, which enables the measurement of longer distances.

S-RE(SP)DOR sequences take the same form as their non-symmetry-based counterparts, however, with a $\pi/(4\sqrt{2})$ slower dephasing rate.³⁷ For instance, in the case of S-REDOR, equation 3 is replaced with:

$$\frac{\Delta S}{S_0} = 1 - \frac{f}{4\pi} \int_0^{2\pi} \int_0^\pi \cos\left(\frac{\pi D\langle S \rangle \tau_{\text{rec}}}{2} \sin 2\beta \sin \alpha\right) \sin \beta d\alpha d\beta \quad (6)$$

One of the great benefits of using this style of dipolar coupling measurement is the ease with which one can predict RE(SP)DOR dephasing curves in multispin systems. For instance, if there are multiple sites that have overlapping chemical shifts, the final RE(SP)DOR dephasing curve is simply the average of those from each of the individual sites, assuming they have comparable transverse relaxation rates.

Simulating the RE(SP)DOR data from a multispin system containing multiple recoupled spins is slightly more involved but can nevertheless be done without reverting to expensive spin dynamics simulations. Dipolar interactions are effectively recoupled independently and as such the total dephasing is simply the product of the dephasing generated by individual spin pairs. For instance, in the case of a REDOR experiment we have:³⁸

$$\frac{\Delta S}{S_0} = 1 - \frac{f}{8\pi^2} \int_0^{2\pi} \int_0^\pi \int_0^{2\pi} \prod_{i=1}^N \cos(2\sqrt{2}D\langle S \rangle \tau_{\text{rec}} \sin 2\beta_j \sin \alpha_j) \sin \beta d\alpha d\beta d\gamma. \quad (7)$$

In equation 7 α_j and β_j represent the orientation of internuclear vector j relative to the MAS rotation axis while α , β , and γ relate the orientation of the entire spin system to the rotor frame. α_j and β_j are functions of α , β , and γ . Using the derivation of Goetz and Schaefer,³⁸ $\sin 2\beta_j \sin \alpha_j$ is rewritten to:

$$\sin 2\beta_j \sin \alpha_j = 2(x \sin \beta \cos \alpha + y \sin \beta \sin \alpha + z \cos \beta)(x(\cos \gamma \sin \alpha - \cos \beta \cos \alpha \sin \gamma) + y(\cos \gamma \cos \alpha - \cos \beta \sin \alpha \sin \gamma) + z(\sin \gamma \sin \beta)) \quad (8)$$

where:

$$x = \sin \theta_j \cos \varphi_j, \quad (9)$$

$$y = \sin \theta_j \sin \varphi_j, \quad (10)$$

$$z = \cos \theta_j \quad (11)$$

and θ_j and φ_j are the polar angles that relate the internuclear vector j to the molecule frame. Expressions 7-11 therefore enable the rapid calculation of REDOR dephasing curves involving very large numbers of recoupled nuclei. It is worth noting also that a good first approximation to the dephasing curve in such a system can be obtained by using equation 5 and adjusting the value of D to root-sum-squares of all the recoupled dipolar interactions affecting the particular detected nucleus.³⁹⁻⁴³

Given that 2-spin REDOR (or RESPDOR) dephasing curves always take the same form, the REDOR dephasing for a particular combination of f , $\langle S \rangle$, D , τ_{rec} , and dipolar recoupling sequence can be quickly determined with the horizontal and vertical rescaling of a precomputed dataset. This is the process used in the INTERFACES program when analyzing atom-to-atom RE(SP)DOR data, which is distinguished from surface-to-atom RE(SP)DOR data. For atom-to-atom RE(SP)DOR data involving numerous recoupled nuclei, INTERFACES uses the root-sum-squares dipolar coupling value, which should be very accurate for representing the initial rise of the RE(SP)DOR curve but may fail to reproduce the long-time behavior of the experiment.

Surface-to-atom REDOR refers to experiments that recouple nuclei on a surface-supported moiety to *all* the spins of a given isotope from the support. Examples would include $^{13}\text{C}\{^{27}\text{Al}\}$ RESPDOR experiments performed on an Al_2O_3 -supported organic species^{22,28,44} or $^{13}\text{C}\{^{29}\text{Si}\}$ REDOR experiments for SiO_2 -supported species.²³ These are inherently multispin processes and it is in fact often necessary to include upwards of 100 recoupled nuclei in order to converge the dephasing curves.²² INTERFACES uses pre-computed libraries of $\Delta S/S_0$ vs. distance away from the support surface and τ_{rec} to avoid repeating the expensive computations. The libraries are stored externally, which enables for the easy addition of new support materials.

3. The INTERFACES Program

On a basic level, INTERFACES modifies input starting structures, compares the agreement between these structures and the provided REDOR data, and either accepts or rejects a structure based on whether it meets the given acceptance criteria. To determine whether a structure is deemed acceptable, a χ^2 metric is used. A χ^2 value is calculated for each of the REDOR dephasing curves using the following expression:^{23,45}

$$\chi_i^2 = \sum_{\tau_{\text{rec}}} \frac{(\Delta S/S_{0,i,\text{expt}} - \Delta S/S_{0,i,\text{calc}})^2}{(\Delta S/S_{0,i,\text{expt}})^2} \quad (12)$$

where i refers to the i^{th} REDOR curve. Note that $\Delta S/S_0$ is superior for this purpose, over the sometimes-used S/S_0 , because it emphasizes the initial rise of the RE(SP)DOR curves. If a search over the conformational space is performed and the lowest value of χ_i^2 (best agreement) is found to be $\chi_{i,\text{min}}^2$, then a threshold χ_i^2 value ($\chi_{i,\text{max}}^2$) can be determined for an arbitrary confidence interval of CI using the following expression.⁴⁵

$$\chi_{i,\text{max}}^2 = \left(2(\text{erf}^{-1}(CI))^2 + 1 \right) \chi_{i,\text{min}}^2 \quad (13)$$

INTERFACES will only accept structures that are simultaneously within the experimental uncertainty of all provided RE(SP)DOR data. Note that Equation 13 has another useful feature, namely, that datasets with lower signal-to-noise will generally feature more scatter and a higher $\chi_{i,\text{min}}^2$ value. As such the fitting will deemphasize these datasets in favor of those of higher quality. This can be seen in several of the examples in section 5 where a wider fan of RE(SP)DOR fits are observed for curves with the largest scatter.

The structure determination process used in INTERFACES is summarized in Figure 2. To minimize the recomputation of REDOR dephasing levels and χ^2 values, INTERFACES begins by creating χ_i^2 vs. distance tables. In cases where there are multiple recoupled nuclei a two-dimensional table is created where the second dimension is either the second distance, when there are only 2 recoupled nuclei, or the standard deviation in a Gaussian distribution of distances, when there are 3 or more recoupled spins. In our trials, we found minimal differences in the fitted curves between the discrete and distributed models involving 3 or more spins, with the exception of bimodal distributions where the initial rise is well-predicted, but not the plateau. The distributed model dramatically reduces the computational cost and memory usage for the calculation of the χ_i^2 tables when large numbers of spins are detected.

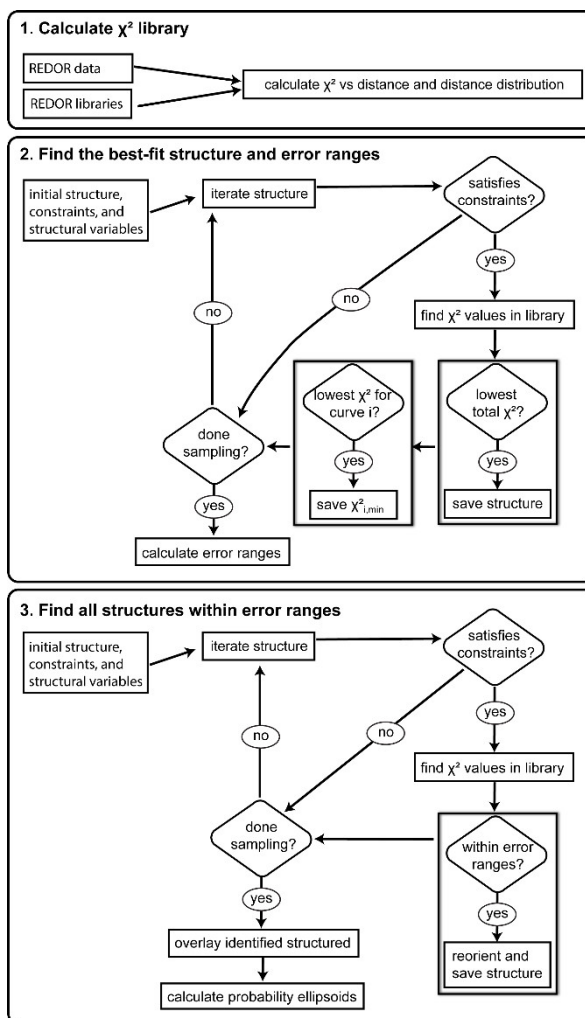


Figure 2. Flowchart describing the data analysis and structure determination process.

Next, the program loads the starting structure, which is provided as a mol2 file. The mol2 file format is used due to its simplicity, ability to handle overlays of multiple structures, and the fact that it stores not only the atomic coordinates but also the bonding network. An input file tells the program what structural elements to iterate and these are surveyed to find 1) the best-fit structure and 2) all the $\chi_{i,min}^2$ values. Once this search is complete, the best-fit structure is saved, and the error ranges for all REDOR curves are calculated using equation 13. This structure search is repeated a second time to find all the structures that agree with the experimental data (within the provided CI , see equation 13). These structures are then combined to generate a structure overlay, as has been used in prior surface 3D structure determinations.^{21,23,24} The overlay is also converted into ORTEP-like probability ellipsoids that are more familiar to most chemists and also less unwieldy when the number of structures is large.

The probability ellipsoids are calculated using the algorithm described by Fyfe and Brouwer.^{46,47} The center of the ellipsoids is simply the mean coordinates (\bar{x}), where the coordinates of a single model are denoted as x_i . An ellipsoids is represented by a second-rank tensor, U . The

principal components of this tensor are the mean-squared deviations (MSD) along their eigenvectors. The MSD along the direction of vector \mathbf{v} is calculated using the following expression.

$$\text{MSD} = \sum_a \frac{(\mathbf{v} \cdot (\mathbf{x}_a - \bar{\mathbf{x}}))^2}{n} \quad (14)$$

To determine the first eigenvector of the tensor, we define a coordinate system $(\mathbf{i}, \mathbf{j}, \mathbf{k})$ and rotate the probe vector \mathbf{k} using two polar angles, β and γ .

$$\mathbf{k}' = \mathbf{R}(0, \beta, \gamma) \mathbf{k} \quad (15)$$

A brute search of β and γ is performed to determine the vector with the largest MSD for this atom. The second eigenvector is found by fixing β and γ and applying a third rotation with an angle of α over which a linear search is again performed to determine the direction with the second largest MSD.

$$\mathbf{j}' = \mathbf{R}(\alpha, \beta, \gamma) \mathbf{j} \quad (16)$$

Finally, the last eigenvector is obtained directly as:

$$\mathbf{i}' = \mathbf{R}(\alpha, \beta, \gamma) \mathbf{i} \quad (17)$$

The \mathbf{U} tensor is then obtained by rotating a diagonal matrix (\mathbf{Q}) having the MSD eigenvalues along the diagonal with the determined values of α , β , and γ .

$$\mathbf{U} = \mathbf{R}(\alpha, \beta, \gamma) \cdot \mathbf{Q} \cdot \mathbf{R}^{-1}(\alpha, \beta, \gamma) \quad (18)$$

The process is repeated for each atom and the results are saved in a crystallographic information file that can be read by most crystallography programs to plot the probability ellipsoids.

4. INTERFACES Input File

The various input file keywords that are supported by INTERFACES are tabulated in Tables 1-3. Table 1 summarizes how to provide INTERFACES with the initial guess structure, using the `structure` keyword, as well as how to provide the program with RE(SP)DOR data. Importantly, the structure must be organized such that the support surface is defined by the $z=0$ plane. REDOR data must be stored as a 2-column text file with the first column being the total recoupling time (τ_{rec} , see Figure 1) in seconds and the second being $\Delta S/S_0$. The user specifies if this is intramolecular (i.e. atom-to-atom) or surface-to-atom RE(SP)DOR data as well as the plateau of the curve (f). $\langle S \rangle$ is assumed to be equal to 1.0, unless it is specified using the `order_parameter` keyword. If the data includes some surface-REDOR data, then it is also necessary to specify the support using the `support` keyword. The program will look for the surface-REDOR libraries with the following structure: `support_element.txt`, for instance, the `29SiO2_C.txt` file contains the $^{13}\text{C}\{^{29}\text{Si}\}$ REDOR library for a carbon atom situated over a ^{29}Si -enriched silica surface. It is best to avoid datapoints with very low values of $\Delta S/S_0$ (below 5% of the plateau value) as these are likely to be overfitted.

Following the declaration of a REDOR dataset, the lists of detected and recoupled spins must be specified using the `detected_spins` and `recoupled_spins` keywords. Note that

a surface-REDOR dataset does not require the declaration of recoupled spins. If the detected nuclei are either ^1H or ^{19}F , a S-RE(SP)DOR experiment is assumed. If the recoupled nuclei are quadrupolar, a RESPDOR experiment is assumed. The most popular nuclear isotopes are assumed in cases where a given element has multiple NMR-active isotopes; for instance, ^{15}N and not ^{14}N . At present, if a different isotope is desired, the source code must be altered. More specifically, the functions `RDD_1A()` and `spin()` in the `REDOR_data.hpp` file, which specify the relative gyromagnetic ratios and spin quantum numbers, would need to be updated.

Table 1. Keywords to specify the structure and REDOR data

<code>structure filename</code>	specifies the filename of the initial structure in a *.mol2 format
<code>support name</code>	specifies the name of the support used (ex. 29SiO2, 27Al2O3) ^a
<code>intramolecular-REDOR filename f</code>	specifies the filename for an intramolecular REDOR curve organized as a 2-column text file with recoupling time in the first column (in seconds) and $\Delta S/S_0$ in the second. The <code>detected_spins</code> and <code>recoupled_spins</code> need to be specified immediately after. The value of f , the contribution factor for the REDOR curve, is also given here.
<code>surface-REDOR filename f</code>	specifies the filename for a surface to atom REDOR curve organized as a 2-column text file with time in the first column (in seconds) and $\Delta S/S_0$ in the second. The <code>detected_spins</code> need to be specified immediately after. The <code>support</code> must be specified. The value of f , the contribution factor for the REDOR curve, is also given here.
<code>detected spins atom₁ atom₂ ... atom_N</code>	a list of the atom indices for the detected nuclei contributing to a given REDOR curve
<code>recoupled spins atom₁ atom₂ ... atom_N</code>	a list of the atom indices for the recoupled nuclei affecting a given intramolecular REDOR curve. Note that if there are multiple recoupled spins, the program will use the root-sum-squares dipolar coupling constant and assume a single recoupled spin.
<code>order_parameter curve_index <S></code>	Specifies that REDOR data from the curve <code>curve_index</code> (curves are indexed in the order that they appear in the input file) is affected by dynamics, with the dipolar coupling reduced by the order parameter <code><S></code> . Note that this can also be used to alter the rate of RESPDOR dephasing in the event that the quadrupolar nucleus is incompletely saturated.

^aThe provided 29SiO2 and 27Al2O3 surface-REDOR libraries were calculated using the amorphous silica surface model of Comas-Vives,^{23,48} and a 110 terminated $\gamma\text{-Al}_2\text{O}_3$ structure.²² A probe nucleus was placed above the surface and its RE(SP)DOR curves were calculated as a function of the distance to the topmost ^{29}Si or ^{27}Al layer, while considering the interactions to the closest 100 surface nuclei. Instructions and code are provided on the github repository for the generation of additional surface-REDOR libraries.

Table 2 lists the various constraints that can be used to limit the structural calculation. This includes structural constraints obtained from other data (for instance EXAFS) such as distance ranges between atoms or between an atom and the surface, and angle and dihedral ranges. It is also

possible to exclude structures with atoms within a minimum distance from one another, or the surface, such that they collide.

A maximum cutoff RMSD value (`cutoff_rmsd`) between a structure and the best-fit structure can be specified to potentially exclude a different conformer from the calculation of the probability ellipsoids. All structures that agree with the experimental data are nevertheless provided.

Experimental agreement is calculated using equations 12 and 13 with the *CI* provided as a percentage with the `confidence_level` keyword.

Table 2. Keywords to specify certain structural constraints.

<code>confidence_level</code> <i>CI</i>
specifies the confidence level used in percent (ex. one standard deviation corresponds to 68 %, default is 90 %)
<code>cutoff_rmsd</code> <i>RMSD</i> (Å)
specifies a maximum rmsd from the structure of best-fit to use in the creation of the structure overlay (default is 2.5 Å)
<code>surface_collision_distance</code> d_{\min} (Å)
specifies the closest distance to the surface that an atom will be allowed to occupy. (default is 1.5 Å) Atoms situated exactly on the surface (i.e. 0 Å) are ignored.
<code>interatomic_collision_distance</code> d_{\min} (Å)
specifies the closest distance that two non-bonded atoms can be from one another (default is 1.5 Å)
<code>max_structures</code> $N_{\text{structures}}$
maximum number of structural solutions. (default is 1000)
<code>distance_constraint</code> $atom_1$ $atom_2$ d_{\min} (Å) d_{\max} (Å)
limits the distance between atoms with indices $atom_1$ and $atom_2$ to between d_{\min} and d_{\max}
<code>angle_constraint</code> $atom_1$ $atom_2$ $atom_3$ θ_{\min} (°) θ_{\max} (°)
limits the angle between atoms with indices $atom_1$, $atom_2$, and $atom_3$ to between θ_{\min} and θ_{\max}
<code>dihedral_constraint</code> $atom_1$ $atom_2$ $atom_3$ $atom_4$ φ_{\min} (°) φ_{\max} (°)
limits the dihedral angle between atoms with indices $atom_1$, $atom_2$, $atom_3$, and $atom_4$ to between φ_{\min} and φ_{\max}
<code>surface_distance_constraint</code> $atom_1$ d_{\min} (Å) d_{\max} (Å)
limits the distance between $atom_1$ and the surface plane to between d_{\min} and d_{\max}

Finally, Table 3 lists the various structural variables that can be searched in the structure determination. These are also depicted in Figure 3. There are three functions (`z_distance`, `rotate_x`, `rotate_y`) that affect the entire molecule and can be useful for probing the orientation of adsorbed molecules on a support. The last three (`revolve`, `stretch`, `bend`) affect only a subset of the molecule. Which atoms are affected by the structural modification is defined by the bonding network, which is treated as a directed chemical graph.⁴⁹ All bonded atoms that are situated beyond the last listed atom in the string, for example $atom_2$ in the `stretch` and `revolve` functions, are moved, while the $atom_1$ end of the molecule remains static. Rotations

are performed according to the procedure described by Parsons *et al.*⁵⁰ Note that the atoms in the string do not need to be bonded (see example in section 5.2). The `z_distance`, `stretch`, and `bend` functions require the specification of a range, while the `rotate` and `revolve` functions perform full 360° rotations. It is still nevertheless possible to restrict dihedral angles using constraints (see example in section 5.1). Importantly, the ranges specified in the structural modifications are not absolute values but rather relative changes. For instance, if a bond angle in the starting structure is 100° and it should be searched from 80° to 120°, then the θ_{\min} and θ_{\max} values would be -20° and 20°.

Table 3. Keywords to specify the structural variables.

<code>z_distance</code> $d_{z,\min}$ (Å) $d_{z,\max}$ (Å) N_{steps}
translate the entire molecule away from the surface from $d_{z,\min}$ to $d_{z,\max}$ in N_{steps} steps
<code>rotate_x</code> N_{steps}
rotate the entire molecule about the x axis in N_{steps} steps.
<code>rotate_y</code> N_{steps}
rotate the entire molecule about the y axis in N_{steps} steps.
<code>revolve</code> $atom_1$ $atom_2$ N_{steps}
specifies that the bond between $atom_1$ and $atom_2$ is rotatable and to sample it in N_{steps} . The $atom_2$ side of the bond is rotated while the $atom_1$ side is kept fixed. Atoms need not be bonded to use this function.
<code>stretch</code> $atom_1$ $atom_2$ d_{\min} (Å) d_{\max} (Å) N_{steps}
increase the distance between $atom_1$ and $atom_2$ from d_{\min} to d_{\max} in N_{steps} steps. The $atom_2$ side of the bond is moved away while the $atom_1$ side is kept fixed. Atoms need not be bonded to use this function.
<code>bend</code> $atom_1$ $atom_2$ $atom_3$ θ_{\min} (°) θ_{\max} (°) N_{steps}
bends the angle formed by $atom_1$, $atom_2$, and $atom_3$ from θ_{\min} to θ_{\max} in N_{steps} steps. The $atom_3$ side of the bond is rotated while the $atom_1$ side is kept fixed. Atoms need not be bonded to use this function.

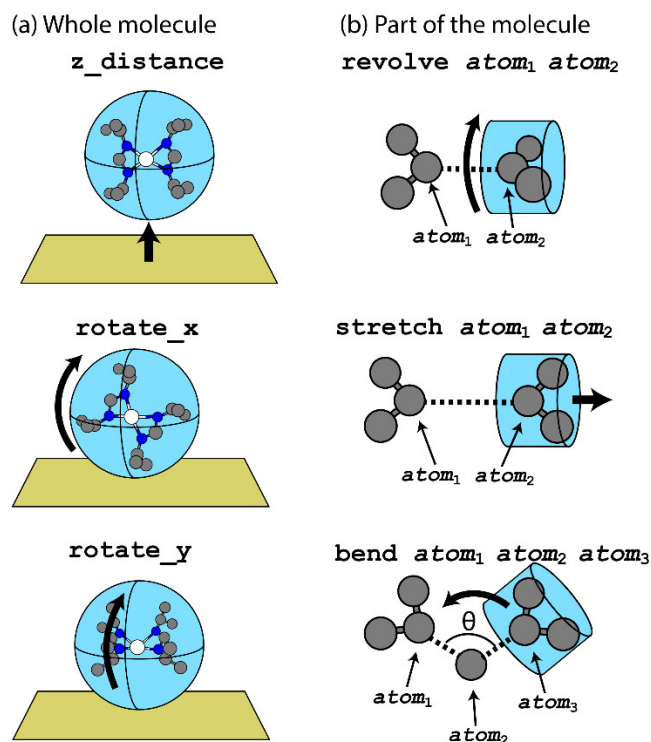


Figure 3. Pictorial description of the six types of structural modifications supported by INTERFACES. Certain operations affect the entire molecule (a) or only a part of it (b).

5. Examples

This section applies INTERFACES to replicate five structure determinations from prior studies. Most of INTERFACES' features are used in these examples, which should help future users in writing their input files and solving new surface structures with the program. All the files from the examples described here are available from the Github repository.

5.1. Surface-Tethered Zn Complex

The first example we will cover is a surface-tethered Zn phenanthroline, originally described in reference 23. The molecular structure is drawn in Figure 4a where all the atoms are numbered in accordance with their order in the mol2 file which describes the starting structure. Nine surface-to-atom $^{13}\text{C}\{^{29}\text{Si}\}$ REDOR curves were measured, the support is a ^{29}Si -enriched mesoporous silica. The REDOR data are shown in Figure 4b, together with the fitted ranges output by INTERFACES following the structure determination.

The input file for the structure determination identifies the name of the starting mol2 file, the support, and the *CI*.

```
structure Zn-phen.mol2
support 29SiO2
confidence_level 95
```

We note that the molecule has 4 rotatable bonds that need to be sampled, between atoms 2 and 3, 3 and 4, 4 and 5, and 8 and 21 (see structure in Figure 4a). These bonds are sampled in 36 steps, corresponding to 10° increments.

```
revolve 2 3 36
revolve 3 4 36
revolve 4 5 36
revolve 8 21 36
```

We then reduce the surface collision distance to 1.3 Å so that the leading silicon site is not thought to collide with the surface. We also constrain the dihedral angle between atoms 2 and 21 to restrict the solution to one of the two possible conformers.

```
surface_collision_distance 1.3
dihedral_constraint 1 2 21 15 -180 0
```

The input file ends with the declaration of the nine different REDOR datasets, and the detected atoms associated with each of the curves (labelled on Figure 4b). Given that the recoupled atoms are from the support, they do not need to be declared. The value of f is set to 1.0 for all nine curves.

```
surface-REDOR Zn-curve1.txt 1.0
detected_spins 2

surface-REDOR Zn-curve2.txt 1.0
detected_spins 4

surface-REDOR Zn-curve3.txt 1.0
detected_spins 15 9 18

surface-REDOR Zn-curve4.txt 1.0
detected_spins 13 19

surface-REDOR Zn-curve5.txt 1.0
detected_spins 11 17

surface-REDOR Zn-curve6.txt 1.0
detected_spins 14 20

surface-REDOR Zn-curve7.txt 1.0
detected_spins 10 16

surface-REDOR Zn-curve8.txt 1.0
detected_spins 6

surface-REDOR Zn-curve9.txt 1.0
detected_spins 25 29
```

Providing INTERFACES with this input file, the starting mol2 structure, and the nine REDOR files leads to the structure determination shown in Figure 4c. The program outputs both

a combined mol2 file with all the various structural solutions overlaid onto the best-fit structure along with a conversion of this file to probability ellipsoids. All the images of the structures shown in this article were generated by exporting the structures to the ray tracing program POV-Ray using Diamond.

INTERFACES also produces a comma-delimited file with the REDOR curves simulated using the best-fit structure in addition to the ranges of fitted curves from the various models in the structure overlay.

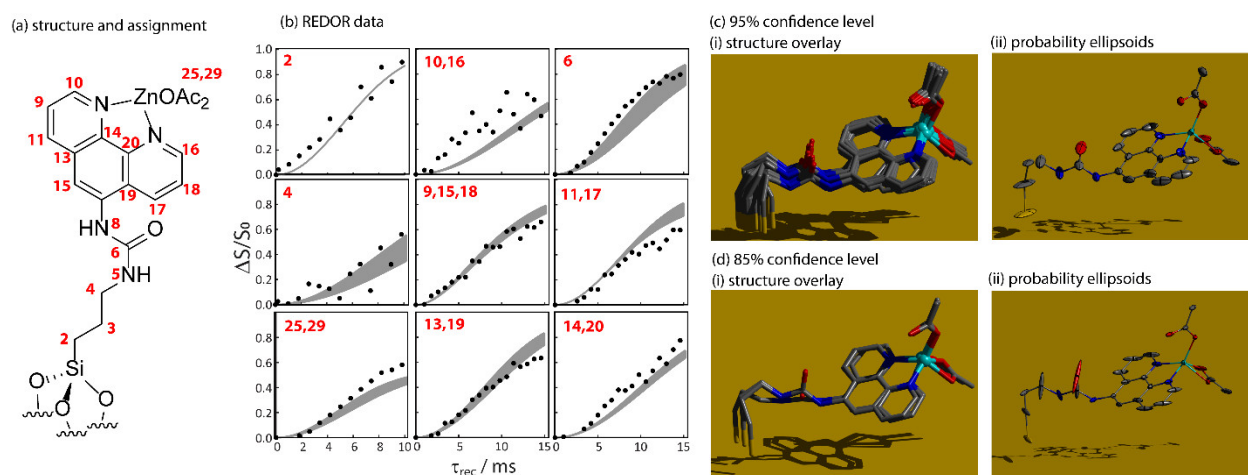


Figure 4. Structure determination of the supported Zn phenanthroline complex with the molecular structure shown in (a); sites are numbered in accordance with their indices in the mol2 file. (b) Experimental $^{13}\text{C}\{^{29}\text{Si}\}$ REDOR curves; shaded areas show the range of simulated curves found in structures within a 95% confidence level. Structures determined at the 95% (c) and 85% (d) confidence levels shown as structure overlays (i) as well as using probability ellipsoids (ii).

Figure 4d shows the impact of reducing the confidence level from 95% to 85%. Doing so narrows the fitting criteria and produces a tighter structure overlay with smaller probability ellipsoids. This easily allows the user to probe the precision of the determined atomic coordinates. It is important to remember, however, that the precision of the fit will depend on the structural variables and constraints that are provided to the program. In addition, note that INTERFACES assumes a single surface structure and that the ellipsoids represent the uncertainties on this fit, although unusually large uncertainties may indicate the presence of multiple surface sites.

5.2. Grafted Sc Complex

The second example covers the structure solution of the Sc amidinate complex from references 23 and 51. This structure can be solved using two different approaches, which we will cover in turn to show two ways that INTERFACES input files can be constructed. In the first approach we define the complex as floating on the surface without a tether and simply optimize its orientation and conformation. The `z_distance`, `rotate_x` and `rotate_y` keywords are all specified to allow the program to fully reorient the complex. In addition, to this, we sample the N-*i*Pr dihedral angles in 90° increments, which enables us to probe all four potential energy minima. Lastly, we rotate one of the two amidinate ligands along its Sc-C vector to search both

square planar and trigonal bipyramidal structures. This is an example of how the revolve functionality can be used to rotate a moiety about the internuclear vector formed by two nonbonded atoms. Because the complex is reoriented it is only necessary to sample one of the two ligands.

```
z_distance -1 3 41
rotate_x 9
rotate_y 9
revolve 1 13 4
revolve 2 5 4
revolve 3 6 4
revolve 11 14 4
revolve 12 15 4
```

We also specify a `cutoff_rmsd` value of 1.5 Å to prevent the program from confusing symmetry-related atoms when calculating the probability ellipsoids. The structure determination and fits of the surface-to-atom REDOR data can be seen in Figure 5b and c.

We can alternatively use an approach akin to that used for the Zn complex (section 5.1) and tether the Sc to the surface using a silanol group (Figure 5d). We can then replace the orientational functions with the `bend` and `revolve` functions, to alter the angle between the O-Sc bond and the support, and reorient the entire complex about its O-Sc bond (`revolve 21 1`). We also need to probe the orientation of the second amidinate ligand and as such we also perform a revolve operation between atoms 1 and 4.

```
bend 20 21 1 -40 40 9
revolve 21 1 9
revolve 1 4 4
revolve 1 13 4
revolve 2 5 4
revolve 3 6 4
revolve 11 14 4
revolve 12 15 4
```

As can be seen in Figure 5d, the same structural solution is found when using the two approaches. The only differences, namely the size of the thermal ellipsoids from the *i*Pr groups closest to the surface are caused by the use of a different `surface_collision_distance` in the second example due to the introduction of the silanol oxygen.

While a $^1\text{H}\{^{45}\text{Sc}\}$ S-RESPDOR dataset was acquired for this complex, shown in Figure 5b along with its fit generated by INTERFACES, this distance is not sensitive to the coordination geometry and was not included in the structure determination. It does, nevertheless, confirm that the ligands are coordinated to the Sc in a bidentate manner.

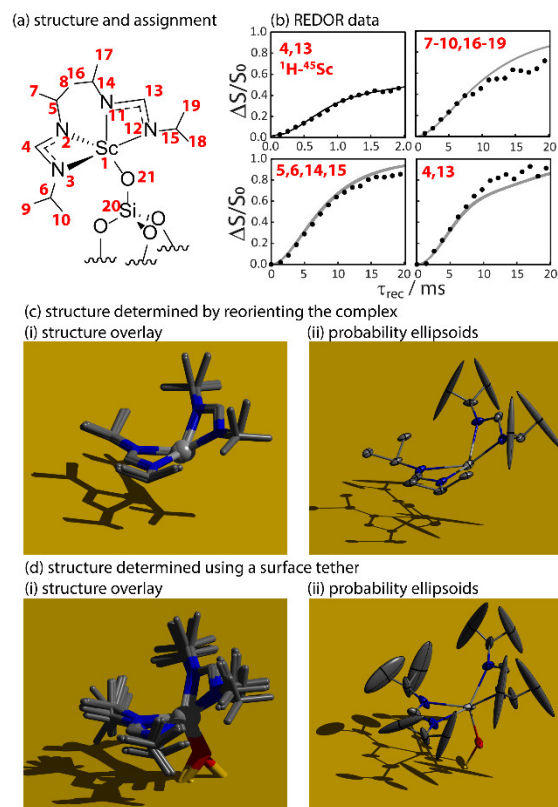


Figure 5. Structure determination of a grafted a Sc amidinate complex with the molecular structure shown in (a); sites are numbered in accordance with indices in the mol2 file. (b) Experimental $^1\text{H}\{^{45}\text{Sc}\}$ S-RESPDOR and $^{13}\text{C}\{^{29}\text{Si}\}$ REDOR curves; shaded areas show the range of simulated curves found in structures within a 90% confidence interval. Structures were determined either by reorienting the complex on the surface (c) or by revolving around and bending a surface tether. Determined structures are shown as an overlay (i) as well as using probability ellipsoids (ii).

5.3. Measuring the Distance Between Surface Species

The next example is taken from reference 27 where the proximity between a surface-supported Pd olefin polymerization catalyst and its perfluorinated Al alkoxide counter anion were probed using a $^1\text{H}\{^{19}\text{F}\}$ S-REDOR experiment (see structure in Figure 6a). Here, INTERFACES is not applied to perform a full structure search, but instead to simply measure the distance between the two complexes. Fitting the data using other software, such as SIMPSON,⁵² is likely to lead to grossly underestimated distances if the multispin nature of the data is not considered. A total of 44 ^1H spins are simultaneously detected and these are all coupled to 27 ^{19}F spins. In such a system, interfaces will calculate the root-sum-squared dipolar coupling constants for each of the ^1H spins coupling to the 27 ^{19}F nuclei and use this value in lieu of the dipolar coupling constant in a single spin pair simulation. The 44 obtained REDOR curves are then averaged to yield the final result.

In this example the input file is quite simple. We built a model with the two complexes on the surface and simply use the `stretch` function to probe the distance between the two. In the initial structure the Pd-Al distance was set to 11 Å and it is probed from 9 to 17 Å in 81 0.1 Å increments. The input file is given below.

```

structure Pd-Al.mol2

stretch 1 122 -2 6 81

confidence_level 90
surface_collision_distance 1.2
cutoff_rmsd 4.0

intramolecular-REDOR SREDOR.txt 1.0
detected_spins 16 17 26 27 40 46 48...
recoupled_spins 135 136 137 138 139 140...

```

The long lists of detected and recoupled spins were truncated. The *CI* is specified to be 90% and at this confidence level the Pd-Al distance is determined to be 11 ± 1 Å. This range of distances is visually depicted in Figure 6c using probability ellipsoids. The experimental S-REDOR data is fitted very well to this range in distances, as shown in Figure 6b.

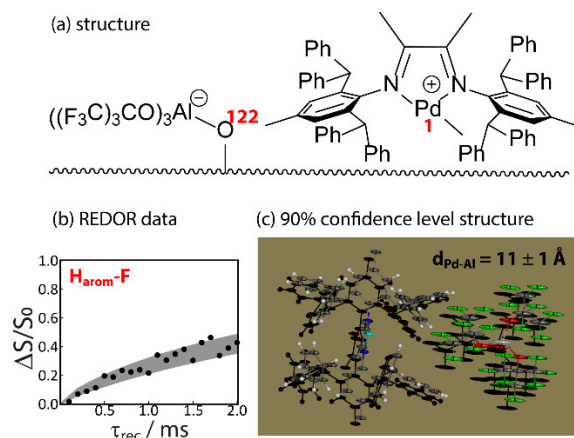


Figure 6. (a) Structure of a silica-supported Pd olefin polymerization catalyst. The ionic Pd complex is charge balanced by a perfluorinated aluminum alkoxide anion. (b) $^1\text{H}\{^{19}\text{F}\}$ S-REDOR curve measured for the 44 aromatic protons coupling to the 27 ^{19}F spins from the counter anion. (c) Determined structure optimizing only the Pd-Al distance.

5.4. Pt NHC Complex

We next reproduce the structure determination of a supported Pt NHC complex (structure in Figure 7a), first solved in reference 21. Unlike the examples in sections 5.1 and 5.2, this structure determination uses exclusively atom-to-atom $^{13}\text{C},^{29}\text{Si}\{^{15}\text{N}\}$ REDOR data. A total of eight REDOR datasets are specified, see Figure 7b. The NMR measurements are sensitive to four dihedral angles, which are sampled in 10° increments.

```

revolve 23 18 36
revolve 22 3 36
revolve 3 4 36
revolve 4 5 36

```

The values for f were measured using the REDOR curves from bonded atoms.²¹ The determined structure is shown in Figure 7c as both an overlay as well as probability ellipsoids. Note that an alternative structure determination approach for this sample could be to manually fit the REDOR data and define the experimental ranges of distances directly using distance constraints instead of relying on INTERFACES to fit the data.

It is possible to further narrow the fit by using the Pt EXAFS data that Berruyer, *et al.* measured which showed that there was a 2.7 Å Pt-O contact (Figure 7d). This EXAFS result can be included in the fit through the use of a distance constraint.

```
distance_constraint 18 19 2.6 2.8
```

In their structure determinations²¹ Berruyer, *et al.* manually probed the Si-Si distance between the two moieties in discrete increments, with values of 3.17 Å, 4.50 Å, and 5.59 Å. These values were taken from a density functional theory model of the amorphous silica surface,⁵³ however, on an amorphous solid nearly any internuclear distance between these sites should be possible. The `stretch` function can be used to accomplish a similar goal and systematically probe the distance between the two silicon atoms.

```
stretch 22 23 -1 2 4
```

From this fit, we obtain a Si-Si distance of 4.7 ± 1.2 Å. This broad distribution of distances agrees with the statements made in the 2017 paper that the distance is ill-defined and likely highly variable. In other words, equally good fits are obtained with a very wide distribution of this Si-Si distance.

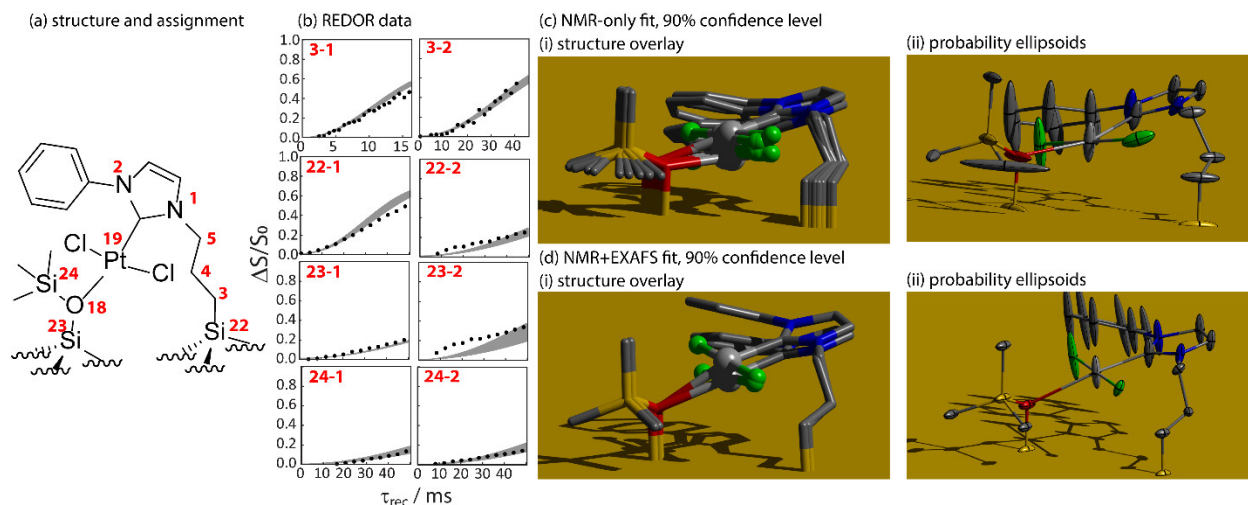


Figure 7. Structure determination of the supported Pt NHC complex with the molecular structure shown in (a); sites are numbered in accordance with indices in the mol2 file. Experimental $^{13}\text{C}\{^{15}\text{N}\}$ and $^{29}\text{Si}\{^{15}\text{N}\}$ REDOR curves; shaded areas show the range of simulated curves found in structures within a 90% confidence interval. Structures determined by using only REDOR data (c) or by using both REDOR data and constraints to limit the Pt coordination environment (d) are shown as structure overlays (i) as well as using probability ellipsoids (ii).

5.5. Grafted Dynamic Zr complex

The last example covers the structure determination of a Zr alkoxide complex^{23,54} (Figure 8a) using $^{13}\text{C}\{^{29}\text{Si}\}$ REDOR data with the complex grafted to ^{29}Si -enriched silica. Using a $^{13}\text{C}\{^1\text{H}\}$ dipolar recoupling experiment the complex was shown to remain very dynamic at 100 K, with both the methyl and tert-butyl groups rotating at a rate that is faster than the timescale of the dipolar couplings. Only two REDOR curves are measured for this complex, as there are only two chemically-distinct sites, and INTERFACES' handling of spectral overlap is key to extracting the structural information from the data. Because the *t*Bu groups are rotating,²³ and that the Zr-O-C angles are nearly 180° ,⁵⁵ the structure determination is defined by varying the angle between the O-Zr bond and the surface, and probing the orientation by revolving the whole complex about the O-Zr bond.

```
bend 19 1 2 -60 60 13
revolve 2 3 36
```

Note that the `bend` operation employs a ghost atom (Gh) to maintain the Zr-O-Si bond angle.⁵⁵ Ignoring dynamics, the best fit is given by the red curves in Figure 8a, corresponding to the structure solution in Figure 8c. As can be seen the quality of the fit for the methyl groups is sub-optimal, likely because of the dynamics that they experience. If we reduce the dipolar interactions that are felt by these atoms using a $\langle S \rangle$ value of 0.7 a better fit is obtained (Figure 8b, grey), and the complex adopts a slightly different conformation (Figure 8d).

```
order_parameter 1 0.7
```

Note that in the above string we specify that the order parameter for the first REDOR curve listed in the input file is 0.7. The order parameter for the second curve is assumed to be 1.0, which is the default. The ability to alter the dipolar scaling factor using the `order_parameter` keyword, in addition with the option to change the contribution factor for different curves, could also be applied to fit other types of data, such as transfer of population double-resonance (TRAPDOR)^{56,57} dephasing curves, by first calculating the relative dipolar scaling factor using a spin dynamics simulation, such as SIMPSON.⁵²

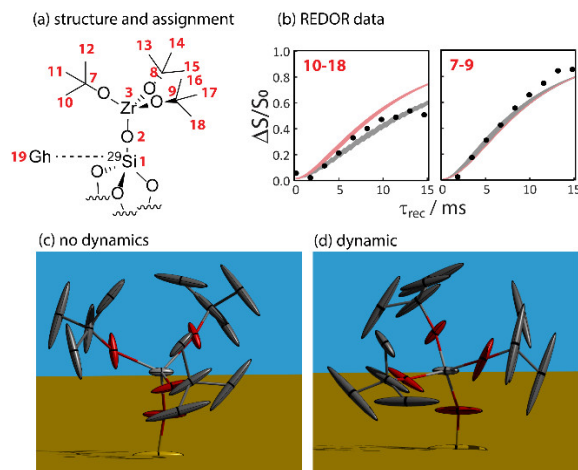


Figure 8. Structure determination of a grafted Zr tert-butoxide complex with the molecular structure shown in (a); sites are numbered in accordance with indices in the mol2 file. (b)

Experimental $^{13}\text{C}\{^{29}\text{Si}\}$ REDOR curves; shaded areas show the range of simulated curves found in structures within a 95% confidence interval with the inclusion of dynamics (grey) as well as in a static model (red). Determined structures are shown assuming no dynamics (c) as well as compensating for the *t*Bu rotation (d).

6. Conclusions

We have presented a new open-source program called INTERFACES for the structure determination of surface sites using RE(SP)DOR dipolar recoupling data in addition to constraints. INTERFACES allows the user to freely alter distances, angles, dihedrals, in addition to a molecule's orientation on the support and automatically compares those structures to multispin REDOR data, either between atoms, or between an atom and the spins in the support. An error analysis is performed to provide structure overlays and thermal ellipsoids at arbitrary levels of precision. This automatic fitting and error analysis can also be used for the rapid fitting of multispin REDOR curves, as shown in section 5.3 where the distance between two surface complexes was measured. Five example structure determinations were covered to emphasize the flexibility of the software. The examples are freely accessible, together with the source code, on a Github repository.

Acknowledgements

We would like to thank Dr. Pierrick Berruyer for sharing his data on the Pt NHC complex as well as Rick Dorn for the Pd example. This work was supported by the U.S. Department of Energy (DOE), Office of Basic Energy Sciences (BES), Division of Chemical Sciences, Geosciences, and Biosciences (CSGB), as a part of the Ames National Laboratory catalysis program. J.C. Would like to also thank DOE for funding a Science Undergraduate Laboratory Internship (SULI). Ames National Laboratory is operated for the DOE by Iowa State University under contract no. DE-AC02-07CH11358.

Data Availability

All of the REDOR data, source files, and example input files and structures are available at: <https://github.com/fperras/INTERFACES/>.

References

-
- ¹ P. Serna, B. C. Gates, Molecular Metal Catalysts on Supports: Organometallic Chemistry Meets Surface Science, *Acc. Chem. Res.* 47 (2014) 2612-2620.
 - ² J. D. Pelletier, J.-M. Basset, Catalysis by Design: Well-Defined Single-Site Heterogeneous Catalysts, *Acc. Chem. Res.* 49 (2016) 664-677.
 - ³ C. Copéret, A. Comas-Vives, M. P. Conley, D. P. Estest, A. Fedorov, V. Mougel, H. Nagaie, F. Núñez-Zarur, P. A. Zhizhko, Surface Organometallic and Coordination Chemistry toward Single-Site Heterogeneous Catalysts: Strategies, Methods, Structures, and Activities, *Chem. Rev.* 116 (2016) 323-421.

-
- ⁴ C. Copéret, F. Allouche, K. W. Chan, M. P. Conley, M. F. Delley, A. Fedorov, I. B. Moroz, V. Mougel, M. Pucino, K. Yamamoto, P. A. Zhizhko, Bridging the Gap between Industrial and Well-Defined Supported Catalysts, *Angew. Chem. Int. Ed.* 57 (2017) 6398-6440.
- ⁵ M. Samantaray, E. Pump, A. Bendjeriou-Sedjerari, V. D'Elia, J. D. A. Pelletier, M. Guidotti, R. Psaro, J.-M. Basset, Surface organometallic chemistry in heterogeneous catalysis, *Chem. Soc. Rev.* 47 (2018) 8403-8437.
- ⁶ M. K. Samantaray, V. D'Elia, E. Pump, L. Falivene, M. Hard, S. O. Chikh, L. Cavallo, J.-M. Basset, The Comparison between Single Atom Catalysis and Surface Organometallic Catalysis, *Chem. Rev.* 120 (2020) 734-813.
- ⁷ A. Lesage, M. Lelli, D. Gajan, M. A. Caporini, V. Vitzthum, P. Miéville, J. Alauzun, A. Roussey, C. Thieuleux, A. Mehdi, G. Bodenhausen, C. Copéret, L. Emsley, Surface Enhanced NMR Spectroscopy by Dynamic Nuclear Polarization, *J. Am. Chem. Soc.* 132 (2010) 15459-15461.
- ⁸ A. J. Rossini, A. Zagdoun, M. Lelli, A. Lesage, C. Copéret, L. Emsley, Dynamic Nuclear Polarization Surface Enhanced NMR Spectroscopy, *Acc. Chem. Res.* 46 (2013) 1942-1951.
- ⁹ T. Kobayashi, F. A. Perras, I. I. Slowing, A. D. Sadow, M. Pruski, Dynamic Nuclear Polarization Solid-State NMR in Heterogeneous Catalysis Research, *ACS Catal.* 5 (2015) 7055-7062.
- ¹⁰ W.-C. Liao, B. Ghaffari, C. P. Gordon, J. Xu, C. Copéret, Dynamic Nuclear Polarization Surface Enhanced NMR spectroscopy (DNP SENS): Principles, protocols, and practice. *Curr. Opin. Colloid Interface Sci.* 33 (2018) 63-71.
- ¹¹ M. K. Samantaray, J. Alauzun, D. Gajan, S. Kavitake, A. Mehdi, L. Veyre, M. Lelli, A. Lesage, L. Emsley, Evidence for Metal–Surface Interactions and Their Role in Stabilizing Well-Defined Immobilized Ru–NHC Alkene Metathesis Catalysts, *J. Am. Chem. Soc.* 135 (2013) 3193-3199.
- ¹² F. A. Perras, Z. Wang, P. Naik, I. I. Slowing, M. Pruski, Natural Abundance ¹⁷O DNP NMR Provides Precise O–H Distances and Insights into the Brønsted Acidity of Heterogeneous Catalysts, *Angew. Chem. Int. Ed.* 56 (2017) 9165-9169.
- ¹³ T. Kobayashi, I. I. Slowing, M. Pruski, Measuring Long-Range ¹³C–¹³C Correlations on a Surface under Natural Abundance Using Dynamic Nuclear Polarization-Enhanced Solid-State Nuclear Magnetic Resonance, *J. Phys. Chem. C.* 121 (2017) 24687-24691.
- ¹⁴ T. Kobayashi, M. Pruski, Spatial Distribution of Silica-Bound Catalytic Organic Functional Groups Can Now Be Revealed by Conventional and DNP-Enhanced Solid-State NMR Methods, *ACS Catal.* 9 (2019) 7238-7249.
- ¹⁵ Z. H. Syed, D. M. Kaphan, F. A. Perras, M. Pruski, M. S. Ferrandon, E. C. Wegener, G. Celik, J. Wen, C. Liu, F. Dogan, K. I. Goldberg, M. Delferro, Electrophilic Organoiridium(III) Pincer Complexes on Sulfated Zirconia for Hydrocarbon Activation and Functionalization, *J. Am. Chem. Soc.* 141 (2019) 6325-6337.
- ¹⁶ G. Qi, Q. Wang, J. Xu, F. Deng, Solid-state NMR studies of internuclear correlations for characterizing catalytic materials, *Chem Soc. Rev.* 50 (2021) 8382-8399.
- ¹⁷ Z. J. Berkson, M. Bernhardt, S. L. Schlapansky, M. J. Benedikter, M. R. Buchmeiser, G. A. Price, G. J. Sunley, C. Copéret, Olefin-Surface Interactions: A Key Activity Parameter in Silica-Supported Olefin Metathesis Catalysts, *JACS Au*, 2 (2022) 777-786.
- ¹⁸ T. Kobayashi, F. A. Perras, T. W. Goh, T. L. Metz, W. Huang, M. Pruski, DNP-Enhanced Ultrawideline Solid-State NMR Spectroscopy: Studies of Platinum in Metal–Organic Frameworks, *J. Phys. Chem. Lett.* 7 (2016) 2322-2327.

-
- ¹⁹ J. Camacho-Bunquin, M. Ferrandon, H. Sohn, D. Yang, C. Liu, P. A. Ignacio-de Leon, F. A. Perras, M. Pruski, P. C. Stair, M. Delferro, Chemoselective Hydrogenation with Supported Organoplatinum(IV) Catalyst on Zn(II)-Modified Silica, *J. Am. Chem. Soc.* 140 (2018) 3940-3951.
- ²⁰ A. Venkatesh, A. Lund, L. Rochlitz, R. Jabbour, C. P. Gordon, G. Menzildjian, J. Viger-Gravel, P. Berruyer, D. Gajan, C. Copéret, A. Lesage, A. J. Rossini, The Structure of Molecular and Surface Platinum Sites Determined by DNP-SENS and Fast MAS 195Pt Solid-State NMR Spectroscopy, *J. Am. Chem. Soc.* 142 (2020) 18936-18945.
- ²¹ P. Berruyer, M. Lelli, M. P. Conley, D. L. Silverio, C. K. Widdifield, G. Siddiqi, D. Gajan, A. Lesage, C. Copéret, L. Emsley, Three-Dimensional Structure Determination of Surface Sites, *J. Am. Chem. Soc.* 139 (2017) 849-855.
- ²² F. A. Perras, A. L. Paterson, Z. H. Syed, A. J. Kropf, D. M. Kaphan, M. Delferro, M. Pruski, Revealing the Configuration and Conformation of Surface Organometallic Catalysts with DNP-Enhanced NMR. *J. Phys. Chem. C.* 125 (2021) 13433-13442.
- ²³ F. A. Perras, U. Kanbur, A. L. Paterson, P. Chatterjee, I. I. Slowing, A. D. Sadow, Determining the Three-Dimensional Structures of Silica-Supported Metal Complexes from the Ground Up, *Inorg. Chem.* 61 (2022) 1067-1078.
- ²⁴ R. Jabbour, M. Renom-Carrasco, K. W. Chan, L. Völker, P. Berruyer, Z. Wang, C. M. Widdifield, M. Lelli, D. Gajan, C. Copéret, C. Thieuleux, A. Lesage. Multiple Surface Site Three-Dimensional Structure Determination of a Supported Molecular Catalyst. *J. Am. Chem. Soc.* 144 (2022) 10270-10281.
- ²⁵ T. Kobayashi, D. Singappuli-Arachchige, I. I. Slowing, M. Pruski, Spatial distribution of organic functional groups supported on mesoporous silica nanoparticles (2): a study by ¹H triple-quantum fast-MAS solid-state NMR, *Phys. Chem. Chem. Phys.* 20 (2018) 22203-22209.
- ²⁶ Y. Chen, S. R. Smock, A. H. FlintGruber, F. A. Perras, R. L. Brutchey, A. J. Rossini, Surface Termination of CsPbBr₃ Perovskite Quantum Dots Determined by Solid-State NMR Spectroscopy, *J. Am. Chem. Soc.* 142 (2020) 6117-6127.
- ²⁷ J. Gao, R. W. Dorn, G. P. Laurent, F. A. Perras, A. J. Rossini, M. P. Conley, A Heterogeneous Palladium Catalyst for the Polymerization of Olefins Prepared by Halide Abstraction Using Surface R₃Si⁺ Species, *Angew. Chem. Int Ed.* 61 (2022) e202117279.
- ²⁸ R. Wang, Z. Zhao, P. Gao, Z. Chen, Z. Gan, Q. Fu, G. Hou, Impact of Adsorption Configurations on Alcohol Dehydration over Alumina Catalysts, *J. Phys. Chem. C* 126 (2022) 10073-10080.
- ²⁹ T. Gullion, J. Schaefer, Rotational-echo double-resonance NMR, *J. Magn. Reson.* 81 (1989) 196-200.
- ³⁰ Z. Gan, Measuring multiple carbon–nitrogen distances in natural abundant solids using R-RESPDOR NMR, *Chem. Commun.* (2006) 4712-4714.
- ³¹ W. Braun, C. Bösch, L. R. Brown, G. Nobuhiro, K. Wüthrich, Combined use of proton-proton overhauser enhancements and a distance geometry algorithm for determination of polypeptide conformations. Application to micelle-bound glucagon, *Biochim. Biophys. Acta*, 667 (1981) 377-396.
- ³² L. Chen, Q. Wang, B. Hu, O. Lafon, J. Trébosc, F. Deng, J.-P. Amoureux, Measurement of hetero-nuclear distances using a symmetry-based pulse sequence in solid-state NMR, *Phys. Chem. Chem. Phys.* 12 (2010) 9395-9405.

-
- ³³ E. Nimerovsky, R. Gubta, J. Yehl, M. Li, T. Polenova, A. Goldbourt, Phase-modulated LA-REDOR: A robust, accurate and efficient solid-state NMR technique for distance measurements between a spin-1/2 and a quadrupole spin, *J. Magn. Reson.* 244 (2014) 107-113.
- ³⁴ M. H. Levitt, Symmetry-based pulse sequences in magic angle spinning solid-state NMR, *Encyclopedia of Magnetic Resonance*, 9 (2002) 165-196.
- ³⁵ A. Brinkmann, A. P. M. Kentgens, Proton-selective ^{17}O - ^1H distance measurements in fast magic-angle-spinning solid-state NMR spectroscopy for the determination of hydrogen bond lengths, 128 (2006) 14758-14759.
- ³⁶ Y. Pan, T. Gullion, J. Schaefer, Determination of C-N Internuclear Distances by Rotational-Echo Double-Resonance NMR of Solids, *J. Magn. Reson.* 90 (1990) 330-340.
- ³⁷ O. Lafon, Q. Wang, B. Hu, F. Vasconcelos, J. Trébosc, S. Cristol, F. Deng, J.-P. Amoureux, Indirect Detection via Spin-1/2 Nuclei in Solid State NMR Spectroscopy: Application to the Observation of Proximities between Protons and Quadrupolar Nuclei, *J. Phys. Chem. A.* 113 (2009) 12864-12878.
- ³⁸ J. M. Goetz, J. Schaefer, REDOR Dephasing by Multiple Spins in the Presence of Molecular Motion, *J. Magn. Reson.* 127 (1997) 147-154.
- ³⁹ M. Bertmer, H. Eckert, Dephasing of spin echoes by multiple heteronuclear dipolar interactions in rotational echo double resonance NMR experiments, *Solid State Nucl. Magn. Reson.* 15 (1999) 139-152.
- ⁴⁰ J. C. C. Chan, H. Eckert, Dipolar Coupling Information in Multispin Systems: Application of a Compensated REDOR NMR Approach to Inorganic Phosphates, *J. Magn. Reson.* 147 (2000) 170-178.
- ⁴¹ M. Bertmer, L. Züchner, J. C. C. Chan, H. Eckert, Short and Medium Range Order in Sodium Aluminoborate Glasses. 2. Site Connectivities and Cation Distributions Studied by Rotational Echo Double Resonance NMR Spectroscopy, *J. Phys. Chem. B.* 104 (2000) 6541-6553.
- ⁴² W. Strojek, M. Kalwei, H. Eckert, Dipolar NMR Strategies for Multispin Systems Involving Quadrupolar Nuclei: $^{31}\text{P}\{^{23}\text{Na}\}$ Rotational Echo Double Resonance (REDOR) of Crystalline Sodium Phosphates and Phosphate Glasses. *J. Phys. Chem. B.* 108 (2004) 7061-7073.
- ⁴³ W. Strojek, H. Eckert, Medium-range order in sodium phosphate glasses: A quantitative rotational echo double resonance solid state NMR study, *Phys. Chem. Chem. Phys.* 8 (2006) 2276-2285.
- ⁴⁴ F. A. Perras, J. D. Padmos, R. L. Johnson, L.-L. Wang, T. J. Schwartz, T. Kobayashi, J. H. Horton, J. A. Dumesic, B. H. Shanks, D. D. Johnson, M. Pruski, Characterizing Substrate-Surface Interactions on Alumina-Supported Metal Catalysts by Dynamic Nuclear Polarization-Enhanced Double-Resonance NMR Spectroscopy, *J. Am. Chem. Soc.* 139 (2017) 2702-2709.
- ⁴⁵ W. H. Press, S. A. Teukolsky, W. T. Vetterling, B. P. Flannery, *Numerical Recipes in C: The Art of Scientific Computing*, 2nd Ed.; Cambridge University Press (1992).
- ⁴⁶ C. A. Fyfe, D. H. Brouwer, Optimization, Standardization, and Testing of a New NMR Method for the Determination of Zeolite Host-Organic Guest Crystal Structures, *J. Am. Chem. Soc.* 128 (2006) 11860-11871.
- ⁴⁷ C. A. Fyfe, J. S. J. Lee, Solid-State NMR Determination of the Zeolite ZSM-5/ortho-Xylene Host-Guest Crystal Structure, *J. Phys. Chem. C.* 112 (2008) 500-513.
- ⁴⁸ A. Comas-Vives, Amorphous SiO_2 surface models: energetics of the dehydroxylation process, strain, ab initio atomistic thermodynamics and IR spectroscopic signatures, *Phys. Chem. Chem. Phys.* 18 (2016) 7475-7482.

-
- ⁴⁹ R. García-Domenech, J. Gálvez, J. V. de Julián-Ortiz, L. Pogliani, Some New Trends in Chemical Graph Theory, *Chem. Rev.* 108 (2008) 1127-1169.
- ⁵⁰ J. Parsons, J. B. Holmes, J. M. Rojas, J. Tsai, C. E. M. Strauss, Practical Conversion from Torsion Space to Cartesian Space for In Silico Protein Synthesis, *J. Comput. Chem.* 26 (2005) 1063-1068.
- ⁵¹ A. L. Paterson, D.-J. Liu, U. Kanbur, A. D. Sadow, F. A. Perras, Observing the three-dimensional dynamics of supported metal complexes, *Inorg. Chem. Frontiers.* 8 (2021) 1416-1431.
- ⁵² M. Bak, J. T. Rasmussen, N. C. Nielsen, SIMPSON: A General Simulation Program for Solid-State NMR Spectroscopy, *J. Magn. Reson.* 147 (2000) 296-330.
- ⁵³ P. Ugliengo, M. Sodupe, F. Musso, I. J. Bush, R. Orlando, R. Dovesi, Realistic Models of Hydroxylated Amorphous Silica Surfaces and MCM-41 Mesoporous Material Simulated by Large-scale Periodic B3LYP Calculations, *Adv. Mater.* 20 (2008) 4579-4583.
- ⁵⁴ U. Kanbur, G. Zang, A. L. Paterson, P. Chatterjee, R. A. Hackler, M. Delferro, I. I. Slowing, F. A. Perras, A. D. Sadow, Catalytic carbon-carbon bond cleavage and carbon-element bond formation give new life for polyolefins as biodegradable surfactants, *Chem.* 7 (2021) 1347-1362.
- ⁵⁵ K. W. Terry, C. G. Lugmair, T. D. Tilley, Tris(tert-butoxy)siloxy Complexes as Single-Source Precursors to Homogeneous Zirconia- and Hafnia-Silica Materials. An Alternative to the Sol-Gel Method, *J. Am. Chem. Soc.* 119 (1997) 9745-9756.
- ⁵⁶ C. P. Grey and W. S. Veeman, The Detection of Weak Heteronuclear Coupling between Spin 1 and Spin 1/2 Nuclei in MAS NMR; ¹⁴N/¹³C/¹H Triple Resonance Experiments, *Chem. Phys. Lett.* 192 (1992) 379-385.
- ⁵⁷ C. P. Grey, A. J. Vega, Determination of the Quadrupole Coupling Constant of the Invisible Aluminum Spins in Zeolite HY with ¹H/²⁷Al TRAPDOR NMR, *J. Am. Chem. Soc.* 117 (1995) 8232-8242.